sustainability

MDPI

Article

Bio-Mediated Zinc Oxide Nanoparticles through Tea Residue: Ecosynthesis, Characterizations, and Biological Efficiencies

Tamil Elakkiya Mathizhagan [1], Vijayakumar Subramaniyan [1,*], Sangeetha Renganathan [2], Vidhya Elavarasan [1], Prathipkumar Subramaniyan [3] and Sekar Vijayakumar [4]

[1] PG and Research Department of Botany, A.V.V.M. Sri Pushpam College (Autonomous), Bharathidasan University, Poondi 613503, India
[2] Department of Mathematics, A.V.V.M Sri Pushpam College (Autonomous), Bharathidasan University, Poondi 613503, India
[3] National Institute of Technology, Tiruchirappalli 620015, India
[4] Marine College, Shandong University, Weihai 264209, China
* Correspondence: svijaya_kumar2579@rediff.com

Abstract: Recent advances in nanotechnology have placed a major emphasis on environmentally friendly processes that encourage sustainable growth by using moderate reaction conditions and non-toxic precursors. In the present study, a simple, inventive, and affordable green technique was applied to generate bio-augmented ZnO nanoparticles using an aqueous extract of tea residue as a reducing and stabilizing component. Numerous methods, including UV-Vis, XRD, FT-IR, FE-SEM with EDAX and TEM were used to analyze ZnO nanoparticles that were generated. The antimicrobial capabilities of biomediated ZnO nanoparticles against pathogenic organisms were examined using an agar well method. 3-(4,5-dimethylthiazol-2-yl)-2,5-diphenyltetrazolium bromide (MTT assay) and flow cytometry analysis was utilized to explore cytotoxic effects and apoptosis, and methylene blue dye was used to examine photocatalytic activity. The ZnO nanoparticles demonstrated considerable anticancer activity in human lung cancer cells (A549) as well as highly effective antibacterial activity against several different microbial pathogens. Furthermore, the greatest degradation percentage of methylene blue obtained was found to be 86% after 140 min. Therefore, it is concluded that the chosen nanoparticle combination enhanced antimicrobial, anticancer and photocatalytic activities. The combination may represent a useful tool for removing dye pollution from wastewater and, ideally, be used in the pharmaceutical sector to combat lung cancer.

Keywords: biofabricated; zinc oxide nanoparticles; tea residue; antimicrobial; lung cancer; photodegradation

Citation: Mathizhagan, T.E.; Subramaniyan, V.; Renganathan, S.; Elavarasan, V.; Subramaniyan, P.; Vijayakumar, S. Bio-Mediated Zinc Oxide Nanoparticles through Tea Residue: Ecosynthesis, Characterizations, and Biological Efficiencies. *Sustainability* **2022**, *14*, 15572. https://doi.org/10.3390/su142315572

Academic Editor: Changhyun Roh

Received: 1 November 2022
Accepted: 17 November 2022
Published: 23 November 2022

1. Introduction

Owing to its applications in biology, chemistry, and medicine, the use of nanotechnology has grown significantly over the past ten years [1]. New avenues in nanoscience have been made possible by advancements in this area, notably in biosensing, nanomedicine, drug delivery and gene delivery [2]. One of the distinguishing qualities of nanoparticles that make them so attractive is their high specific surface area ratio [3]. Nanoparticles are more reactive than bulk material even though atoms on the surface are typically more aggressive than those located in the middle [4].

Since the emergence of nanotechnology, several nanoscale devices have been created which utilize a variety of techniques, including physical, chemical and eco-friendly methods. The preferred tool is green nanoparticle synthesis, which involves a simple manufacturing process. The use of hazardous substances, lengthy processing times, high costs, and arduous processes are only some of the downsides of current methods used for the creation of nanoparticles. Due to these limitations, most pertinent research has focused on ecological and rapid synthesis techniques for the creation of nanoparticles [5]. Recently, the attention

of materials scientist has been focused on creating eco-friendly processes for producing nanocomposites. Accordingly, the biosynthesis of nanoparticles, especially when using plant extracts, has been a key development that is recognized as easy, economical and harmless in green chemistry [6].

The development of nanoparticles that are non-toxic, non-polluting and biogenic is the main emphasis of the present investigation. Recent years have seen the successful production of several metal oxide nanoparticles, including Zn, Ag, Mg, Cu, Pt, and Al, using biogenic modes of synthesis for a variety of commercial applications [7]. The II-VI semiconductor family, which includes zinc oxide nanoparticles, exhibits a wide energy gap spectrum at 3.2 eV and greater charge carrier bond energy at 60 meV [8].

As a result of the multiple applications of metal oxide nanoparticles in numerous technical domains, extensive study into these particles has occurred over the last ten years [9]. ZnO nanoparticles are an intriguing class of inorganic materials that provide a variety of advantages. ZnO nanoparticles have potential applications in a range of areas, including catalysis, cosmetics, semiconductors, textiles, electronics, healthcare and chemical sensing [10]. These nanoparticles also have potential medicinal applications in targeted drug administration, wound healing and bioimaging [11]. They are non-toxic and biocompatible and have anticancer, anti-inflammatory and antibacterial activities [12].

Here, we introduce waste tea residue as a long-lasting, moderate and efficient adsorptive material. It is readily accessible in vast quantities throughout the world. Therefore, the goal of the present research was to fabricate ZnO nanoparticles from tea residue and to investigate the antimicrobial, cytotoxic and photocatalytic capabilities of the ZnO nanoparticles.

2. Materials and Methods

2.1. Chemicals

Zinc acetate dehydrate $Zn(C_2H_3O_2)_2.2H_2O$ and all other chemicals and reagents, sodium hydroxide (NaOH) and $2H_2O$ were procured from EMerk in India. Each obtained chemical and reagent's analytical grade permitted its use without further purification.

2.2. Gathering and Processing of Tea Residue Extracts

The tea residue was collected from a street corner tea shop in Thanjavur, completely cleansed with deionized water and dried outside for two days at room temperature before baking for two hours in a hot air oven at 110 °C. The dry tea waste powder was finely ground in a kitchen blender. The resulting tea waste powder was weighed and saved for subsequent use after being strained until the particle size was less than 25 µm.

2.3. Synthesis of Zinc Oxide Nanoparticles

A quantity of 50 mL of tea waste powder extract was added to 0.1 M zinc acetate solution and the mixture was kept in a magnetic stirrer for 30 min at 60 °C. After that, the pH was retained at a value of 8 by injecting a liquid ammonia solution. The solution was filtered using Whatman No. 1 filter paper after progressively becoming colloidal. After obtaining the green-synthesized ZnO, the surplus liquid ammonia was repeatedly washed away with Milli Q water. The resulting pellets were then dried for 2 h in a hot air oven at 80 °C. Powdered ZnO nanoparticles were retained and stored for future investigations (Figure 1).

2.4. Characterizations of ZnO Nanoparticles

The crystallinity of the ZnO nanoparticles was assessed using X-ray diffraction (XRD). The optical characteristics of the ZnO nanoparticles were examined at various wavelengths between 300 and 700 nm using a UV-Vis NIR dual-beam spectrophotometer. Using Fourier transform infrared spectroscopy (FT-IR-Perkin Elmer RX-I Spectrophotometer US), the functional groups of the nanoparticles were investigated. A field emission scanning electron microscope (FE-SEM) was used to study the morphology of the ZnO nanoparticles. The formulation of the ZnO nanoparticles was investigated using an energy-dispersion X-ray

(EDX) technique. Transmission electron microscopy (TEM, Hitachi H-7100) was performed to determine the purity of substances.

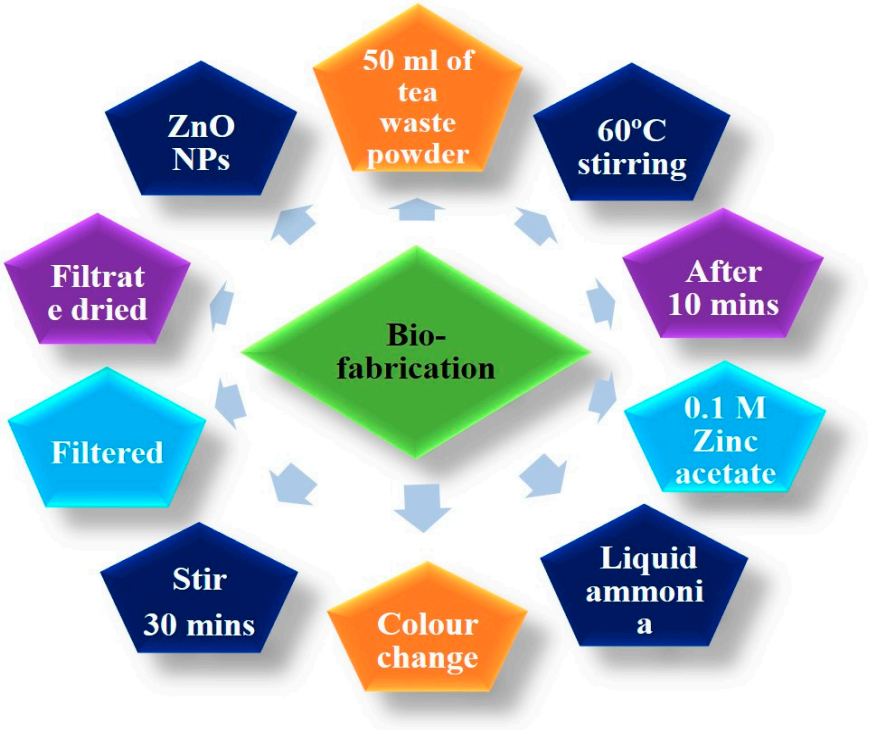

Figure 1. Schematic of the ZnO nanoparticle synthesis process.

2.5. Antimicrobial Efficiencies

An antimicrobial analysis of the fabricated nanoparticles from the aqueous tea residue extract was investigated using a well diffusion technique. The Eumic Analytical Lab and Research Institute, Tiruchirappalli, India, contacted the Microbial Type Culture Collection (MTCC), Chandigarh, India, to obtain Gram + ve (*Staphylococcus epidermidis*, *Enterococcus faecalis*), Gram − ve (*Shigella dysenteriae*, *Salmonella paratyphi*), and fungal samples (*Candida albicans*, *Aspergillus niger*). The organisms were sub-cultured in MHA (Muller–Hinton agar) and SDA (Sabouraud dextrose agar) media at 35 °C and 30 °C, respectively, for the bacterial and fungal cultures. Wells of 6 mm-diameter were used to pierce the MHA and SDA plates. Using a micropipette, a quantity of 20 µL of the material was injected into each well of all the plates. Gentamycin (50 µg), a common antibiotic, and ketoconazole (5 µg) served as the +ve and −ve controls, respectively. The cultures were then maintained to be incubated later at 30 °C for 24–48 h for the bacterial cultures and 37 °C for 72–96 h for the fungal cultures. After incubation, the diameter of the zones surrounding the well was measured (mm). Triplet plates were used to ensure the results.

2.6. Antiproliferation Efficiencies

The NCCS (National Center for Cell Science) in Pune, India, supplied the human lung cancer cell lines (A549); the cells were resequenced in DMEM medium (Dulbecco's Modified Eagle's Medium). Human lung cancer and healthy cell lines were treated in vitro with the fabricated ZnO nanoparticles. The cell cultures were evaluated using 3-(4,5-dimethylthiazol-2-yl)-2,5-diphenyltetrazolium bromide (MTT, Sigma, Aldrich, Mumbai, India). The lung cancer cells (1×10^5 cells/well) were plated and cultured for 24 h in a 24-well plate. The media for the grown cells and various ZnO nanoparticle concentrations were produced and combined. The media for the grown cells and various ZnO nanoparticle concentrations were generated and homogenized. Each well was then filled with 100 µL

(5 µg/mL) with 5% MTT before being maintained at 37 °C for 4 h. A UV-spectrophotometer was used to measure the cell vitality at 570 nm.

2.7. Cell Morphology Examination

By means of a cellular morphology experiment, it was determined whether the ZnO nanoparticles had any effect on the morphology of the human lung cancer cells. A 25 cm^2 culture flask was used to plate the cells, which were labeled with 1×10^6 acridine orange cells. After that, the ZnO NPs were injected into the cells (IC_{50}). Then, the cells were kept in an incubator for 24 h at 37 °C and 5% CO_2. Following trypsinization, the cells were centrifuged, cleaned with ice-cold PBS and stained with acridine orange (1:1 v/v) at a concentration of 100 µg/mL. The developed morphological structures were examined using a fluorescent microscope in the dark, applying the Q-Flora program.

2.8. Flow-Cytometric Study of the Cell Cycle

The A549 cells were centrifuged at 2000 rpm for 5 min with synthesized ZnO nanoparticles after being rinsed with Milli Q water (control) (IC_{50} concentration). The cells were put into suspension in 500 µL ethanol after fixation in 70% cold PBS (phosphate buffer red saline) and incubated for two hours at 20 °C. The cells were then centrifuged once again for five minutes at a speed of 2000 rpm, and the pellet containing the cells was collected. The pellets were treated with 400 mL of propidium iodide (PI) and 100 mL of RNase. The cells were incubated for 30 min in the dark at 4 °C before analysis of the sample. The cell cycle was examined utilizing a flow cytometer (a Beckman culture flow cytometer) with an excitation wavelength of 488 nm [12].

2.9. Photocatalytic Efficiencies

To test the photocatalytic activity of the fabricated ZnO NPs, we generated 20 ppm of methylene blue dye in 50 mL of deionized water. The starting solution (5 mL) was separated and the remaining solution of 25 mg (0.025 g) ZnO-NPs catalyst was added to 45 mL of dye solution. To maintain the adsorption–desorption equilibrium, the solution was exposed to UV light for 20 min, with samples taken every 20 min. The samples were centrifuged at 10,000 rpm for 15 min to eliminate the catalyst; the dye degradation was monitored using a UV-visible spectrophotometer. The formula below was used to compute the deteriorated dye's percent degradation [9]; here C_0 and A_0 represent the dye's starting concentrations, and C_t and A_t represent the concentrations over a period of time.

$$\% = \frac{C_o - C_t}{C_o} \times 100$$

$$\% = \frac{A_o - A_t}{A_o} \times 100$$

2.10. Statistical Analysis

A triplet of each experiment was conducted. Using one-way analysis of variance, the antibacterial activity of the samples was compared to that of conventional antibiotics. The findings were presented as mean ± standard errors.

3. Results and Discussion

3.1. Optical Study

The typical peak of the pure ZnO nanoparticles, which have an absorption maximum of 365 nm, is shown in Figure 2. Peak-widening was in good accord with the published literature between 320 and 380 nm [13,14]. The absence of an additional peak in the spectrum indicated that the ZnO NPs were extremely pure and crystalline [15].

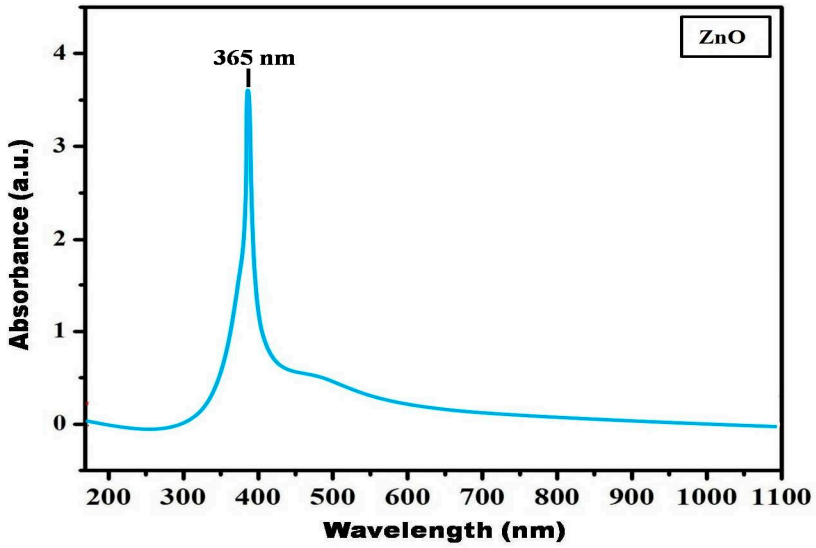

Figure 2. UV-Vis spectrum of ZnO nanoparticles.

3.2. XRD

The spectrum of green-fabricated ZnO nanoparticles is shown in Figure 3. Prominent peaks were identified that were in fair concordance with the published literature from the International Center of Data Diffraction card (JCPDS-36–1451). The peaks in the ZnO nanoparticles spectrum appeared with 2 θ between 20 and 70, with observable diffraction angles of 32.7°, 35.1°, 37.9°, 48.3°, 57.8°, 71.5°, 76.9°, 77.4° and 79.7° that indicated crystal size, and prominent ZnO (hkl) index values of (100), (002), (101), (102), (110), (103), (200), (112) and (201). The average size of the nanoparticles was determined using the Debye–Scherrer equation, which was found to be between 30 and 40 nm [16]. The results indicated that the fabricated ZnO sample was highly crystalline and had a hexagonal wurtzite crystalline structure, determined using the Bragg equation, λ=2$d$sinθ; these XRD results were consistent with previous research [17]. The zinc oxide nanoparticles in the sample were visible in the usual XRD pattern. The produced metal oxide nanoparticle XRD pattern showed a high level of crystallinity in the samples with diffraction angles that conformed to a distinctive face-centered cubic structure. XRD patterns were analyzed to assess the peak intensity, location and breadth [18].

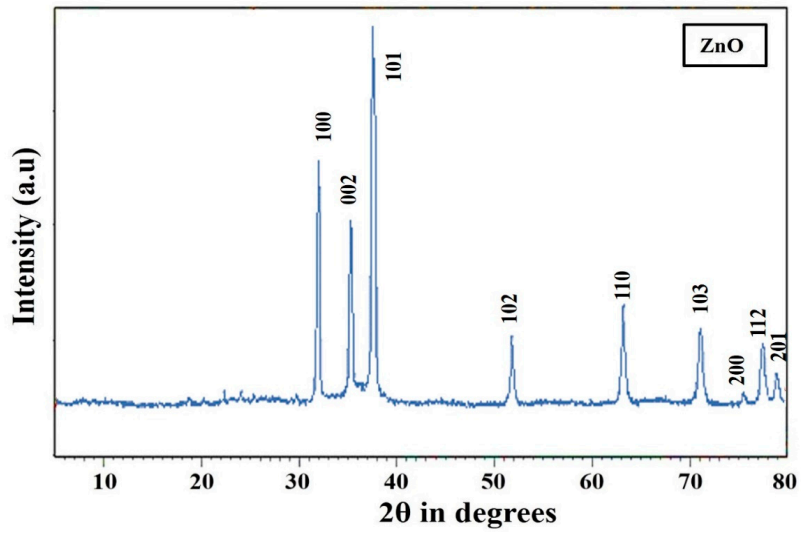

Figure 3. XRD pattern of ZnO nanoparticles.

3.3. FT-IR Analysis

Using FT-IR spectrometry, it was possible to identify the functional groups associated with the synthesis of the ZnO NPs (Figure 4). The existence of octahedral sites was suggested by a peak in the vicinity of 3726 cm^{-1} [19]. According to Anbuvannana et al. [20], the steep peak at 3426 cm^{-1} is caused by C-H stretching vibrations of carboxylic acid and hydroxyl stretch vibrations, while the peak at 3240 cm^{-1} is formed by the existence of a hydroxyl group (-OH-) in the oxidized oil [21]. The band at 10 cm^{-1} indicated the carboxylic group (-COOH) of the minority polymer [22], while the peak from 1092 cm^{-1} demonstrated the existence of C-O-C bonds [23]. C-H bending (C=C-H) was responsible for the peak at 608 cm^{-1} [24].

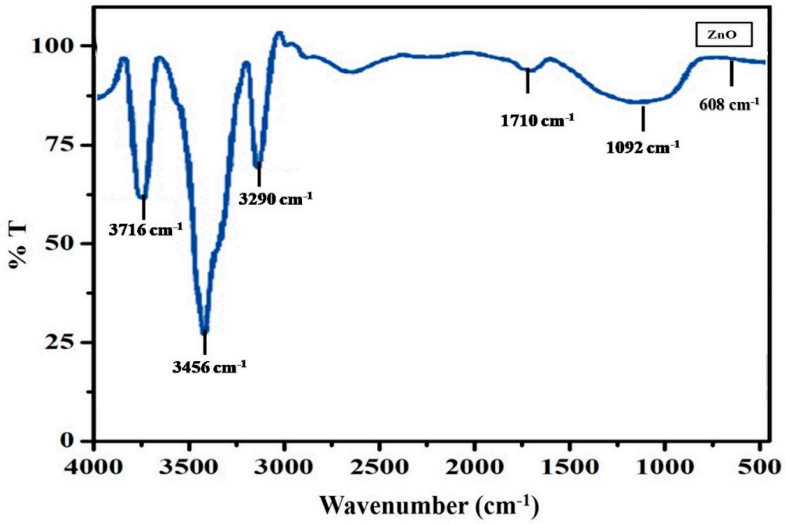

Figure 4. FT-IR spectrum of ZnO nanoparticles.

3.4. FE-SEM with EDX

The morphology of the fabricated ZnO nanoparticles was explored using FE-SEM analysis, as shown in Figure 5a. An agglomerated micrograph made it easy to see that the green ZnO nanoparticles were spherical in form. The average particle size of the ZnO nanoparticles was 29 nm. Figure 5b depicts a histogram of the particle size distribution of the produced ZnO nanoparticles. EDAX was also used to investigate the purity and elemental composition of the ZnO nanoparticles. The only elements found in the sample were Zn and O, as shown in Figure 5c.

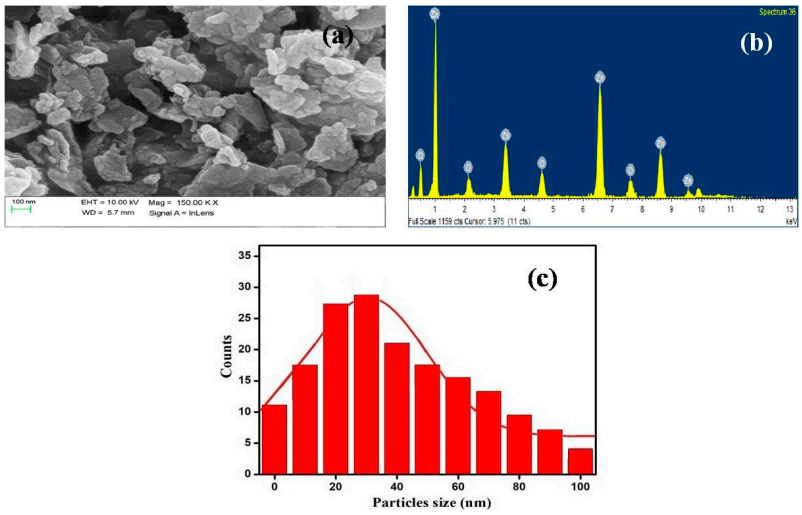

Figure 5. (**a**) FE-SEM micrograph (**b**) EDAX analysis and (**c**) histogram of ZnO nanoparticle distribution.

3.5. TEM

The average particle size of the biosynthesized ZnO nanoparticles, as ascertained by TEM analysis and shown in Figure 6a, was determined to be 27 nm. This was confirmed by the XRD results, which also indicated that the particles were spherical and hexagonal in shape. The SAED pattern, which is shown in Figure 6b, confirmed that the produced ZnO nanoparticles were crystalline. The SAED pattern showed that the produced ZnO nanoparticles were polycrystalline.

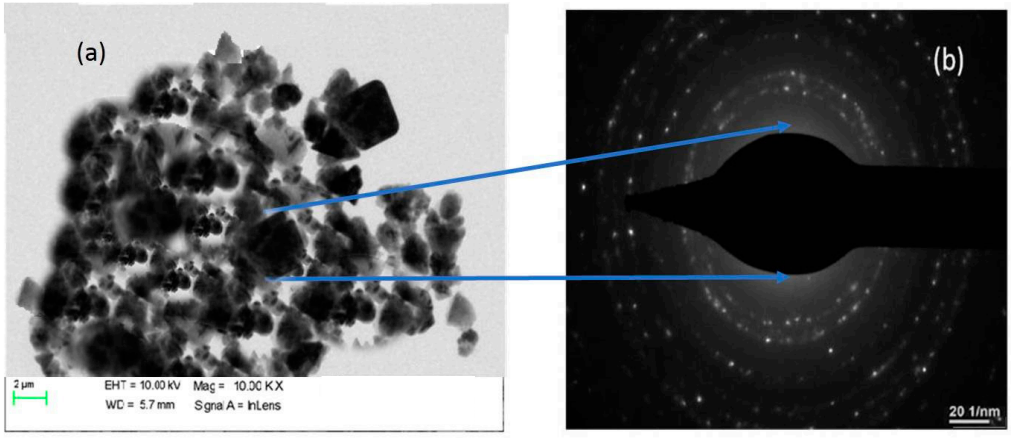

Figure 6. (**a**) TEM micrograph of ZnO nanoparticles (**b**) SAED pattern of ZnO nanoparticles.

3.6. Antimicrobial Efficiencies

The antimicrobial ability of the fabricated ZnO nanoparticles was assessed for several plant diseases caused by Gram + ve, Gram − ve bacteria, and fungal strains. This was compared to the effects of tea waste extract, zinc acetate and Gentamycin (50 µg), for each of which the growth of all the examined microbial strains was suppressed. It is evident from the results provided in Table 1 that the ZnO nanoparticles exhibited a broad spectrum of antimicrobial effects. *S. epidermidis* (25 mm) showed the largest inhibitory zones, followed by *E. faecalis* (22 mm), *S. paratyphi* (20 mm) and *S. dysenteriae* (19 mm). The ZnO nanoparticles showed considerable antifungal potentials for all the test species when compared to the conventional antifungal Nystatin (50 µg) for antifungal activity (Table 1).

Table 1. Antimicrobial activity.

S. No.	Name of the Organisms	Zone of Inhibition (µg/mL^{-1}) [a]			
		Tea Waste Extract	Zinc Acetate	ZnO NPs	Control
1.	*Staphylococcus epidermidis*	13 ± 1.18	14 ± 1.80	25 ± 2.01	12 ± 1.08
2.	*Enterococcus faecalis*	12 ± 0.99	13 ± 1.89	22 ± 1.90	11 ± 1.07
3.	*Shigella dysenteriae*	10 ± 0.86	11 ± 0.75	19 ± 0.69	10 ± 1.12
4.	*Salmonella paratyphi*	11 ± 1.02	12 ± 1.57	20 ± 1.11	13 ± 0.80
5.	*Candida albicans*	9 ± 0.55	10 ± 1.94	18 ± 1.20	14 ± 0.76
6.	*Aspergillus niger*	8 ± 0.66	9 ± 0.44	16 ± 0.99	10 ± 0.50

[a] Mean values of three triplicates ± standard deviation; Tea waste extract, zinc acetate, ZnO NPs—zinc oxide nanoparticles, control–gentamycin (50 µg).

A previous study reported that ZnO nanoparticles were more effective towards Gram + ve bacteria than Gram − ve bacteria [25]. The differences in sensitivity between Gram + ve bacteria and Gram − ve bacteria may be due to differences in their morphology. The outer lipopolysaccharide membrane of Gram − ve bacteria prevents chemical antibacterial agents from passing through the cell wall. Gram + ve bacteria, on the other hand, are more vulnerable because they only have an exterior layer of peptidoglycan, which is ineffective as a permeability barrier. As a result, Gram-negative bacteria have

more intricate cell walls than Gram-positive bacteria, which serve as a diffusion barrier and reduce their susceptibility to antibacterial drugs [26]. Scientists have proposed several potential bactericidal pathways for ZnO NP interactions with bacteria. Some have suggested that smaller NPs produce Zn^{2+} because they more easily penetrate cells and have a more reactive surface. The effect of the release of Zn^{2+} from ZnO NPs, which is known to inhibit several bacterial cell functions, including active transport, bacterial metabolism and enzyme activity, ultimately resulting in the death of bacterial cells, represents one of the main recognized antimicrobial mechanisms because of the toxic properties of Zn^{2+} [27]. The electrostatic binding of ZnO NPs to the bacterial cell membrane is another potential mechanism for the antibacterial action of these nanoparticles. This contact might compromise the integrity of the bacterial cell and damage the membrane plasma structure, allowing the internal contents to seep out, leading to cell death [28].

The antibacterial activity of ZnO NPs is significantly influenced by the oxidative stress they create. Zn^{2+} ions that are created from ZnO interact with respiratory enzymes to limit their activity. It has already been shown that ZnO NPs may disrupt cell membranes and induce ROS. By absorbing Zn^{2+} ions, the bacterial cell membrane, DNA, and mitochondria are irreversibly damaged, which causes oxidative stress, the production of ROS and free radicals that limit the activity of respiratory enzymes, and ultimately cause cell death. Figure 7 provides a schematic illustration of how ZnO NPs eliminate microorganisms [29].

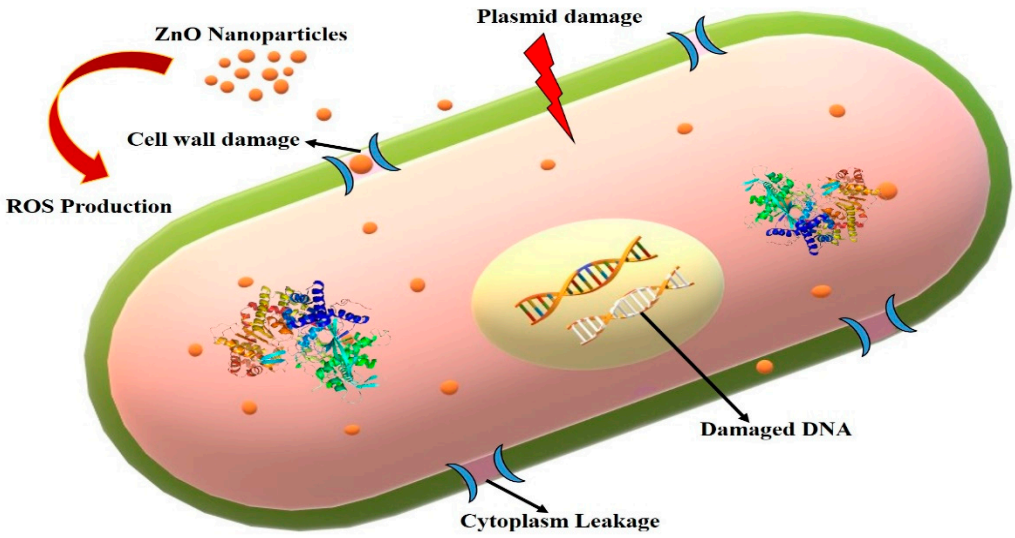

Figure 7. Mechanism of antimicrobial activity in ZnO nanoparticles.

3.7. MTT Assay

The MTT test was employed to measure the cell proliferation of A549 cancer cells at various concentrations (0.78, 15.6, 31.2, 62.5, 125, 250, 500, and 1000 µg/mL) of fabricated ZnO nanoparticles. The ZnO nanoparticles that were created entered the cells significantly after 24 h of exposure, as shown by the IC_{50} cell viability of 40.89% (Figure 8). The results showed that bioproduced ZnO nanoparticles seemed to have an impact on the viability of A549 cells even at the lowest concentrations of the provided samples. These results are consistent with those of Vidhya et al. [12] and Vijayakumar et al. [30] who found that low concentrations of biosynthesized ZnO NPs reduced cell viability. The acridine orange staining of A549 cells is seen in Figure 9. We note that the IC_{50} values were 31.2 µg/mL when ZnO nanoparticles were exposed to 0.1% DMSO. These results are consistent with those of Namvar et al. [31] and Vidhya et al. [12], who showed that treatment with 0.1% DMSO reduced the viability of cancer cells stained with acridine orange by 85%.

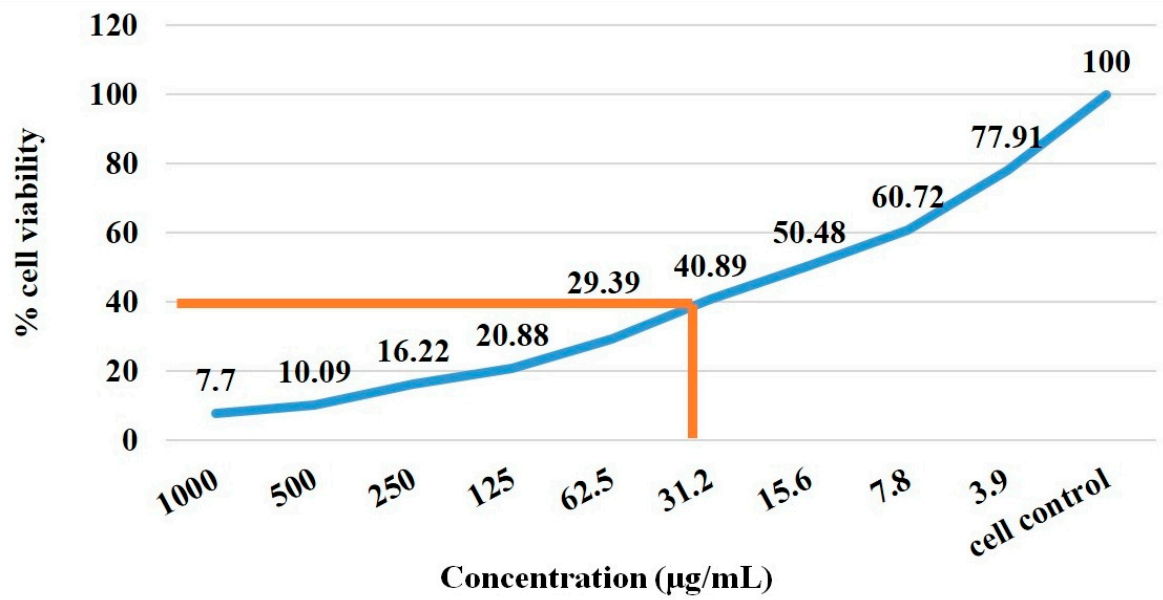

Figure 8. Antiproliferative effect of ZnO nanoparticles using MTT assay.

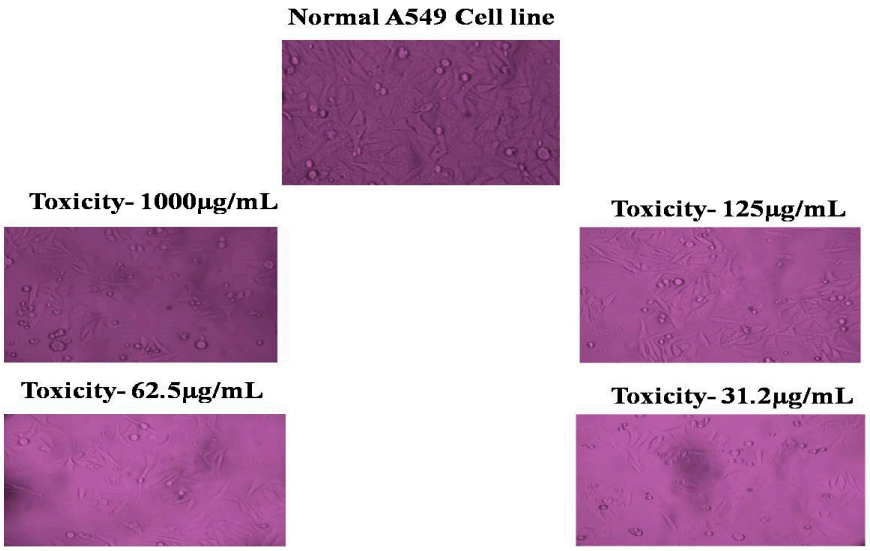

Figure 9. Cytotoxic effect of lung cancer cell line with various concentrations of ZnO nanoparticles.

3.8. Analysis of Cell Cycle by Flow Cytometry

The apoptotic examination of biosynthesized ZnO nanoparticles was further verified using annexin V-FITC/PI dyes and flow cytometry. Figure 10 depicts the cell viability in comparison to the early, late and necrotic stages of apoptosis. Phosphatidyl serine translocation from the plasma membrane's outer layers marks the beginning of apoptosis. The annexin-V bound to phosphatidyl serine is highlighted by blue fluorescence because of the strong affinity of calcium ions. Late apoptosis is characterized by an increase in membrane permeability; the nucleus becomes red as a result of cellular DNA binding by the PI stain. These results are consistent with the findings of past research studies of the cell cycle, showing that the early stages of cell death are induced by manufactured ZnO nanoparticles in a variety of cell lines, including SHSY5Y cells, neuronal Schwann cells and human skin cancer cells [12,32].

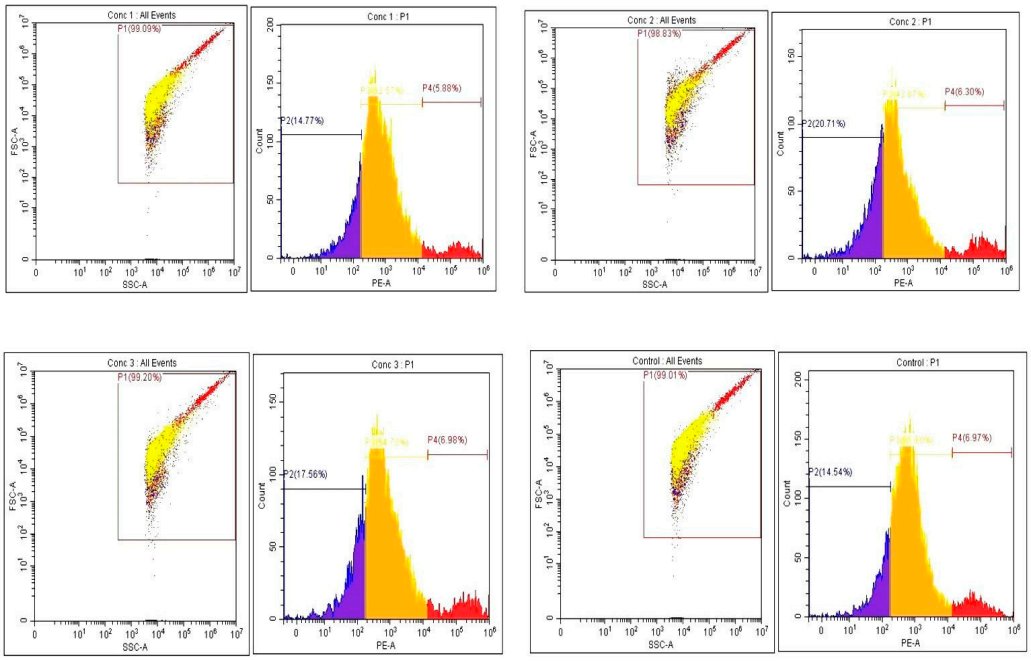

Figure 10. Cell cycle analysis by flow cytometry of ZnO nanoparticles in A549 cells.

3.9. Photocatalytic Efficiencies

The photocatalytic abilities of the as-prepared ZnO NPs were examined for their ability to photodegrade MB in an aqueous solution. Figure 11 depicts the UV-Vis absorption spectra of MB degradation under UV light using ZnO NPs. A sign of MB degradation was the strength of the peak at 463 nm, which was connected to the typical absorption peak of MB and diminished progressively without changing the maximum absorption wavelength. The dye solution with catalyst was agitated for 30 min in the dark to encourage the adsorption–desorption process; it was observed that 2% of the dye adsorbed. Defects in the ZnO NPs were the cause of this. The MB content steadily dropped under UV light once the photocatalyst had been applied. The degrading efficiency of MB was discovered to be 86% after 140 min of irradiation.

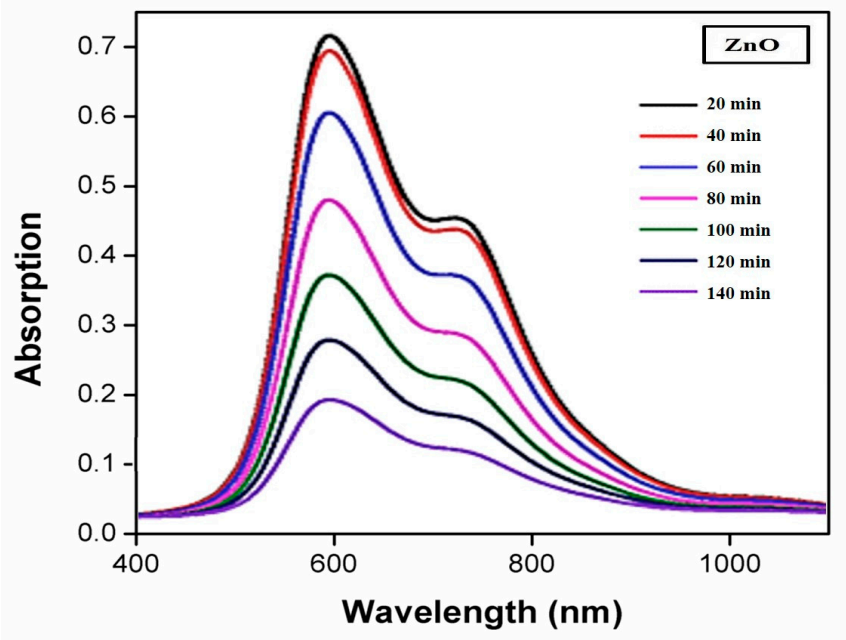

Figure 11. Photodegradation of MB with biofabricated ZnO nanoparticles.

An increase in active sites is responsible for improvement in degradation efficiency, and photocatalysis is better suited to the higher number of photons absorbed by the catalyst. Catalyst concentrations higher than the recommended level may result in aggregation, making the active areas on the catalyst surface inaccessible to light absorption [33,34]. Another factor contributing to lower degradation efficiency is the turbidity of the suspension, which is caused by the scattering effect on the catalytic surface of ZnO NPs, which inhibits photon absorption [35].

ZnO as a semiconductor absorbs light when its band gap value is greater than the value needed to form electron-hole pairs (e-h+). The conduction band of the ZnO nanoparticles receives the dye's electron from its excited state. Excitation may be split into electrons and holes, which may then move to the surface of the catalyst and interact with absorbed species to produce redox reactions. As can be observed, the surface-bound reaction of h+ vb with water resulted in the production of hydroxyl radicals, and the oxygen-dependent choice of e cb resulted in the production of the radical anion (superoxide radicals) (Figure 12).

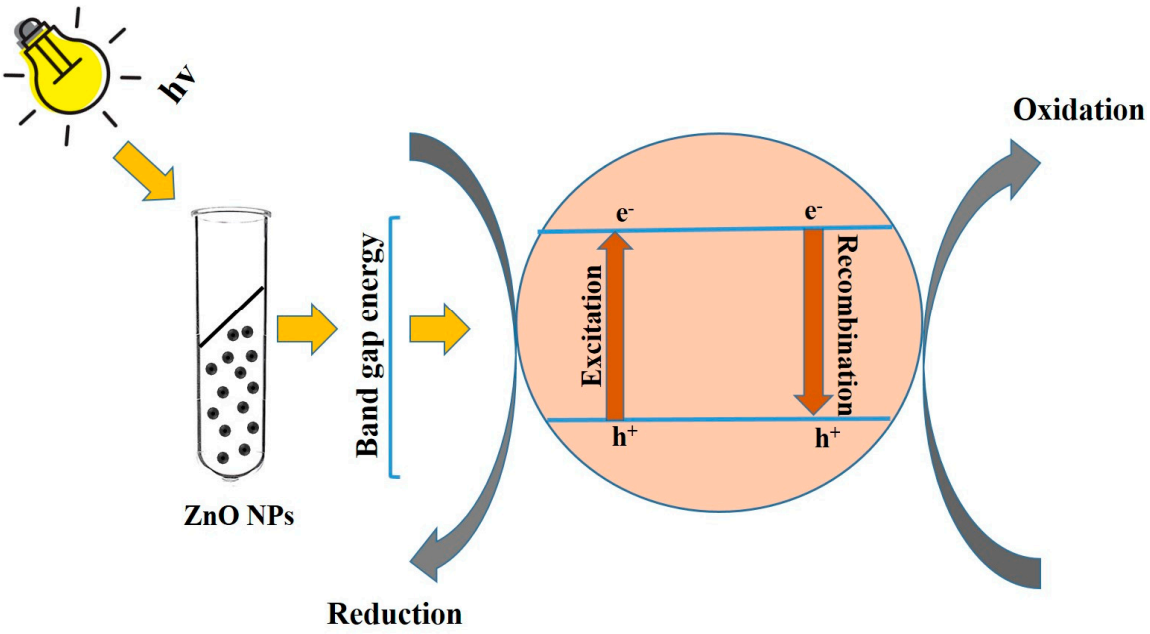

Figure 12. ZnO NPs' generalized mechanism of photodegradation on ZnO NPs.

4. Conclusions

ZnO nanoparticles were synthesized using an environmentally benign, economically feasible process utilizing readily accessible tea residue extract. Applying a variety of analytical methods, biofabricated ZnO nanoparticles were characterized. The results indicated that the biofabricated ZnO nanoparticles exhibited excellent antimicrobial activity. Additionally, the samples produced demonstrated potential to protect A549 cells and outstanding photocatalytic activity, resulting in the reduction of MB by 89%.

Author Contributions: T.E.M. was responsible for sample collection and characterization; V.S. designed the study and monitored the overall process, including writing of the paper—all authors contributed to the final paper; S.R. undertook the analysis of photodegradation; V.E. analyzed microbial activity; P.S. and S.V. analyzed the anticancer activity. All authors have read and agreed to the published version of the manuscript.

Funding: This research was funded by DST-FIST (SR/FST/College-222/2014), DBT-STAR (HRD-11011/18/2022-HRD-DBT).

Institutional Review Board Statement: The study was conducted according to the guidelines of the declaration and approved by the ethics committee of Bharathidasan University, Trichy and AVVM Sri Pushpam College (Autonomous), Poondi, Thanjavur.

Informed Consent Statement: Informed consent was obtained from all subjects involved in the authors.

Data Availability Statement: On behalf of all the authors, the corresponding author states that our data are available upon reasonable request.

Acknowledgments: We sincerely express our thanks to the management of A.V.V.M. Sri Pushpam College (Autonomous), Poondi, for providing us with the necessary facilities and support to carry out this work.

Conflicts of Interest: The authors declared no conflict of interest.

References

1. Samer, B.; Muhammad, A.; Tiziano, T.; Marco, C.; Flavio, R. The History of Nanoscience and Nanotechnology: From Chemical–Physical Applications to Nanomedicine. *Molecules* **2020**, *25*, 112. [CrossRef]
2. Joseph, R.R.; Venkatraman, S.S. Drug delivery to the eye: What benefits do nanocarriers offer? *Nanomedicine* **2017**, *12*, 683–702. [CrossRef] [PubMed]
3. Khan, I.; Saeed, K.; Khan, I. Nanoparticles: Properties, Applications and Toxicities. *Arab. J. Chem.* **2019**, *12*, 908–931. [CrossRef]
4. Ashwini, J.; Aswathy, T.R.; Achuthsankar, S.N. Green synthesis and characterization of zinc oxide nanoparticles using *Cayratia pedata* leaf extract. *Biochem. Biophys. Rep.* **2021**, *26*, 100995. [CrossRef]
5. National Nanotechnology Initiative (NNI). Available online: www.nano.gov (accessed on 22 July 2019).
6. Bala, N.; Saha, S.; Chakraborty, M.; Maiti, M.; Das, S.; Basu, R.; Nandy, P. Green synthesis of zinc oxide nanoparticles using Hibiscus subdariffa leaf extract: Effect of temperature on synthesis, anti-bacterial activity, and anti-diabetic activity. *RSC Adv.* **2015**, *5*, 4993–5003. [CrossRef]
7. Vijayakumar, S.; Krishnakumar, C.; Arulmozhi, P.; Mahadevan, S.; Parameshwari, N. Biosynthesis, characterization and antimicrobial activities of zinc oxide nanoparticles from leaf extract of Glycosmis pentaphylla (Retz.) DC. *Microbpathog* **2018**, *116*, 44–48. [CrossRef]
8. Matinise, N.; Fuku, X.; Kaviyarasu, G.; Mayedwa, K.; Maaza, N. ZnO nanoparticles via *Moringa oleifera* green synthesis: Physical properties & mechanism of formation. *Appl. Surf. Sci.* **2017**, *406*, 339–347. [CrossRef]
9. Faisal, S.; Jan, H.; Shah, S.A.; Shah, S.; Khan, A.; Akbar, M.T.; Rizwan, M.; Jan, F.; Wajidullah; Akhtar, N.; et al. Green Synthesis of Zinc Oxide (ZnO) Nanoparticles Using Aqueous Fruit Extracts of *Myristica fragrans*: Their Characterizations and Biological and Environmental Applications. *ACS Omega* **2021**, *6*, 9709–9722. [CrossRef]
10. Sankapal, B.R.; Gajare, H.B.; Karade, S.S.; Salunkhe, R.R.; Dubal, D.P. Zinc Oxide Encapsulated Carbon Nanotube Thin Films for Energy Storage Applications. *Electrochim. Acta* **2016**, *192*, 377–384. [CrossRef]
11. Cai, X.; Luo, Y.; Zhang, W.; Du, D.; Lin, Y. pH-Sensitive ZnO Quantum Dots-Doxorubicin Nanoparticles for Lung Cancer Targeted Drug Delivery. *ACS Appl. Mater. Interfaces* **2016**, *31*, 22442–22450. [CrossRef]
12. Vidhya, E.; Vijayakumar, S.; Prathipkumar, S.; Praseetha, P.K. Green way biosynthesis: Characterization, antimicrobial and anticancer activity of ZnO nanoparticles. *Gene Rep.* **2020**, *20*, 100688. [CrossRef]
13. Datta, A.; Patra, C.; Bharadwaj, H.; Kaur, S.; Dimri, N.; Khajuria, R. Green synthesis of zinc oxide nanoparticles using *Parthenium hysterophorus* leaf extract and evaluation of their antibacterial properties. *J. Biotechnol. Biomater.* **2017**, *7*, 271–275. [CrossRef]
14. Saravanakkumar, D.; Sivaranjani, S.; Umamaheswari, M.; Pandiarajan, S.; Ravikumar, B. Green synthesis of ZnO nanoparticles using *Trachyspermum ammi* seed extract for antibacterial investigation. *Der. Pharma. Chemica* **2016**, *8*, 173–180.
15. Santhoshkumar, J.; Kumar, S.V.; Rajeshkumar, S. Synthesis of zinc oxide nanoparticles using plant leaf extract against urinary tract infection pathogen. *Resour. Effic. Technol.* **2017**, *3*, 459–465. [CrossRef]
16. Irshad, S.; Salamat, A.; Anjum, A.A.; Sana, S.; Saleem, R.S.Z.; Naheed, A.; Iqbal, A.; Yang, J. Green tea leaves mediated ZnO nanoparticles and its antimicrobial activity. *Cogent Chem.* **2018**, *4*, 1469207. [CrossRef]
17. Agarwal, H.; Kumar, S.V.; RajeshKumar, S. A review on green synthesis of zinc oxide nanoparticles—An eco-friendly approach. *Resour.-Effic. Technol.* **2017**, *3*, 406–413. [CrossRef]
18. Moghaddam, A.B.; Moniri, M.; Azizi, S.; Rahim, R.A.; Ariff, A.B.; Saad, W.Z.; Namvar, F.; Navaderi, M.; Mohamad, R. Biosynthesis of ZnO Nanoparticles by a New Pichia kudriavzevii Yeast Strain and Evaluation of Their Antimicrobial and Antioxidant Activities. *Molecules* **2017**, *22*, 872. [CrossRef]
19. Najma, B.; Khan Kasi, A.; Khan Kasi, J.; Akbar, A.; Bokhari, S.M.A.; Stroe, I.R. ZnO/AAO Photocatalytic Membranes for Efficient Water Disinfection: Synthesis, Characterization and Antibacterial Assay. *Appl. Surf. Sci.* **2018**, *448*, 104–114. [CrossRef]
20. Anbuvannana, M.; Ramesh, M.; Manikandan, E.; Srinivasan, R. Vitex negundo leaf extract mediated synthesis of ZnO nanoplates and its antibacterial and photocatalytic activities. Asian. *J. Nanosci. Mater.* **2018**, *2*, 99–110. [CrossRef]
21. Singh, Y.; Kumar, S.N.; Sharma, A.; Singla, A.; Singh, D.; Abd Rahim, E. Effect of ZnO nanoparticles concentration as additives to the epoxidized Euphorbia Lathyris oil and their tribological characterization. *Fuel* **2021**, *285*, 119148. [CrossRef]

22. Ali, H.A.; Iliadis, A.A.; Mulligan, R.F.; Cresce, A.V.W.; Kofinas, P.; Lee, U. Properties of self-assembled ZnO nanostructures. *Solid-State Electron.* **2002**, *46*, 1639–1642. [CrossRef]
23. Yaqoob, K.; Durrani, S.K.; Mazhar, M.; Jamil, A.; Riaz Khan, M.; Shamraz, F. Low-temperature synthesis of fluorescent ZnO nanoparticles. *Appl. Surf. Sci.* **2010**, *257*, 1756–1761. [CrossRef]
24. Mebrahtu, H.K. Synthesis and characterization of ZnO nanoparticles using aqueous extract of Becium grand forum for antimicrobial activity and adsorption of methylene blue. *Appl. Water Sci.* **2021**, *11*, 45. [CrossRef]
25. Ahmed, A.T.; El-Tras, W.F.; Shaaban, M.; El-Baz, A.F.; Hoda, M.; Mohammed, F.S.; Leon, B. Antibacterial Action of Zinc Oxide Nanoparticles Against Foodborne Pathogens. *J. Food Saf.* **2011**, *31*, 211–218. [CrossRef]
26. Getie, S.; Belay, A.; Reddy, A.R.; Chandra, Z.B. Synthesis and Characterizations of Zinc Oxide Nanoparticles for Antibacterial Applications. *J. Nanomed. Nanotechnol.* **2017**, *s8*, 1–8. [CrossRef]
27. Demissie, M.G.; Sabir, F.K.; Edossa, G.D.; Gonfa, B.A.; Gawdzik, B. Synthesis of Zinc Oxide Nanoparticles Using Leaf Extract of *Lippia adoensis* (Koseret) and Evaluation of Its Antibacterial Activity. *J. Chem.* **2020**, *2020*, 7459042. [CrossRef]
28. Jayaseelan, C.; Abdul Rahuman, A.; Vishnu Kirthi, A.; Marimuthu, S.; Santhoshkumar, T.; Bagavan, A.; Gaurav, K.; Karthik, L.; Bhaskara Rao, K.V. Novel microbial route to synthesize ZnO nanoparticles using *Aeromonas hydrophila* and their activity against pathogenic bacteria and fungi. *Spectrochim. Acta* **2012**, *90*, 78–84. [CrossRef]
29. Insoo, K.; Karthika, V.; Gopinath, K.; Sarinthip, T.; Kambiz, S.; Jongchul, S. ZnO Nanostructures in Active Antibacterial Food Packaging: Preparation Methods, Antimicrobial Mechanisms, Safety Issues, Future Prospects, and Challenges. *Food Rev. Int.* **2022**, *38*, 537–565. [CrossRef]
30. Vijayakumar, S.; Nilavukkarasi, M.; Sakthivel, B. Bio-synthesized zinc oxide nanoparticles for anti-tuberculosis agent: Scientifically unexplored. *Gene Rep.* **2020**, *20*, 100764. [CrossRef]
31. Namvar, F.; Baharara, J.; Mahdi, A.A. Antioxidant and anticancer activities of selected Persian Gulf algae. *Ind. J. Clinic. Biochem.* **2014**, *29*, 13–20. [CrossRef]
32. Xu, W.; Shen, G.; Li, T.; Zhang, Y.; Zhang, T.; Xue, H.; Zuo, W.; Li, Y.; Zhang, D.; Jin, C. Isoorientin induces the apoptosis and cell cycle arrest of A549 human lung cancer cells via the ROS-regulated MAPK, STAT3 and NF-κB signalling pathways. *Int. J. Oncol.* **2020**, *57*, 550–561. [CrossRef]
33. Gavade, N.L.; Kadam, A.N.; Gaikwad, Y.B.; Dhanavade, M.J.; Garadkar, K.M. Decoration of biogenic AgNPs on template free ZnO nanorods for sunlight driven photocatalytic detoxification of dyes and inhibition of bacteria. *J. Mater. Sci. Mater. Electron.* **2016**, *27*, 11080–11091. [CrossRef]
34. Minha, R.; Ajda, K.; Lev, M.; Sonja, S.M.; Martin, S.; Andraz, S. Controlled growth of ZnO nanoparticles using ethanolic root extract of Japanese knotweed: Photocatalytic and antimicrobial properties. *RSC Adv.* **2022**, *12*, 31235–31245. [CrossRef]
35. Gawade, V.V.; Gavade, N.L.; Shinde, H.M.; Babar, S.B.; Kadam, A.N.; Garadkar, K.M. Green synthesis of ZnO nanoparticles by using *Calotropis procera* leaves for the photodegradation of methyl orange. *J. Mater. Sci. Mater. Electron.* **2017**, *28*, 14033–14039. [CrossRef]